Available online at www.sciencedirect.com

ScienceDirect

Procedia IUTAM 10 (2014) 273 – 284

Procedia IUTAM

www.elsevier.com/locate/procedia

23rd International Congress of Theoretical and Applied Mechanics

Nanomechanics of graphene and nanocrystals

Wei Yang*, Hongtao Wang

Institute of Applied Mechanics, Zhejiang University, Hangzhou 310058, China

Abstract

Nanomechanics understandings for nanostructures are critical not only for their integrity concerns but also for their utilization. Attention here is focused on two types of low-dimensional materials, graphene and nanocrystals, with characteristic lengths in nanometers or even angstrom scales. In nanocrystals, the dislocation mechanism is suppressed, and their plasticity is dictated by diffusive atomistic flow along the grain boundaries. Nanomechanics models are developed for the plastic flow and fracture in nanocrystals. Simulations based on micro-structural evolution demonstrate the capability in predicting the brittle versus ductile transition of nanocrystal. To put this mechanism into atomistic images, in-situ tests of nano-crystalline gold were performed under HRTEM. We observe atoms flow along certain atomistic planes of the crack faces to facilitate the advance of the crack. This diffusion assisted mode, along with GB cavitations and cleavage, give a complete spectrum of defect evolutions in nanocrystals.

Aside from the danger of degrading the nanostructures, defects in graphene may serve to enrich its functions. The functioning of pristine graphene is rather limited for exploration. Doping of graphene, however, can be achieved around their defects, such as vacancies and edges. We study the defect creation and evolution in graphene. A two-step method was devised for atomic doping of graphene: the first step consists of creating holes and vacancies in graphene by the bombardment of Au atoms, while the second step consists of doping atoms of various kinds to the edges of the hole, as well as into the atomic vacancies. These doping atoms serve to functionalize the edges and to create catalysts in the form of single atom arrays. The mechanics of graphene is explored by monitoring the atom-resolved tearing in graphenes, and by elucidating the tailoring mechanisms of graphene nano-ribbon. We are able to create a two-dimensional iron film, termed ironene, with the constraining support from the graphene edges. The segregation of metallic clusters on a graphene sheet is also explored.

© 2013 Published by Elsevier Ltd. Open access under CC BY-NC-ND license.
Selection and/or peer-review under responsibility of the Organizing Committee of The 23rd International Congress of Theoretical and Applied Mechanics, ICTAM2012

Keywords: nanomechanics, graphene, nanocrystal

*Corresponding author. *E-mail address*: yangw@zju.edu.cn.

2210-9838 © 2013 Published by Elsevier Ltd. Open access under CC BY-NC-ND license.
Selection and/or peer-review under responsibility of the Organizing Committee of The 23rd International Congress of Theoretical and Applied Mechanics, ICTAM2012
doi:10.1016/j.piutam.2014.01.023

1. Nanomechanics of nanocrystals

Nanocrystalline metals exhibit physical properties different from ordinary polycrystals. The attention is focused on their unique deformation and fracture behaviour. By preparing nanocrystalline Cu of high purity and high density, Lu et al. [1] demonstrated the grain boundary induced superplasticity at room temperature. Equal-axed grains were maintained during the rolling-induced elongation, even at an elongation ratio of 5 100%. The deformation is believed to achieve mainly by accommodated matter that flows via grain boundaries. We adopted a 9-grain cluster model [2–4] to describe the grain boundary induced plastic deformation. The model uses 9 grains to illustrate a self-repeated deformation process, which can be divided into two sub-processes, insertion and rotation, as shown in Fig. 1. The grain arrangement changes from armchair to zigzag in the insertion process, then from zigzag to armchair in the rotation process. The cluster elongates twice of its original length and shrinks to a half of its original width. One-dimensional [2] and three-dimensional constitutive laws [3] were developed whose prediction agreed with the testing data [1].

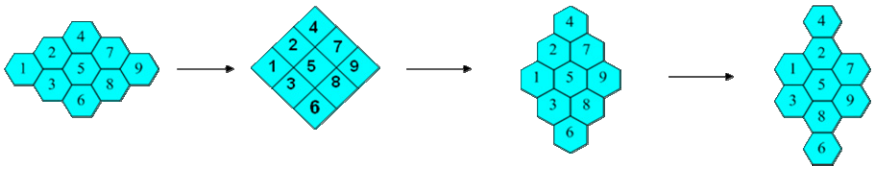

Fig. 1. 9-grain cluster model for the plastic flow of nanocrystals, after Yang and Wang [2]

The highest attainable value for the strength of nanocrystals is another inspiring topic. The introduction of nano-twins may enhance the strength of nanocrystals by blocking the passage of extended dislocations. It was reported that a peak in the maximum strength could be identified at an intermediate twin spacing in nano-twinned NC copper [5]. Molecular dynamics computations [6] elucidated the occurrence of this strength peak. At higher twin-spacing, the blocking effect on dislocation is attenuated; while at lower twin spacing, the dislocation may thread underneath the twin boundaries in a necklace chain fashion. The influence of twin structure for the fracture toughness is carefully examined by Zhou et al. [7] through MD simulations.

Several differences exist between the experiment [5] and the simulation [6]: (1) the mean grain size is in microns in experiment but in tens of nanometers in MD simulation; (2) the strain rate is 6×10^{-3} s^{-1} in experiment but is 2×10^{8} s^{-1} in MD simulation; (3) in contrast to the defect-free twin planes in simulation, the samples in experiment have a sit-in dislocation density of 10^{14} m^{-2} and that may contribute to dislocation nucleation controlled mechanism; (4) the softening mechanism may differ under different orientations.

To explore the last aspect, one may devise a particular orientation shown in the left graph of Fig. 2, where a columnar grain with nano-twins parallel to the loading axis is under investigation. The green lines in the graph denote the grain boundary, the red lines denote the twin boundaries, and the gray atoms represent the perfect FCC copper atoms. Accordingly, the spreading dislocations beneath the twin boundaries are no longer operative. Our simulation indicates that the nano-twinned crystal will strengthen all the way as the twin spacing decreases, as shown in the right graph of Fig. 2.

It is interesting to compare the defect structures under this loading configuration but with different twin spacings. For the case of 5 nm twin spacing, one encounters the situation of confined slip, as shown in Fig. 3. The defects are dominated by threading dislocations in the form of partials. The twin boundaries serve to hinter the threading dislocations.

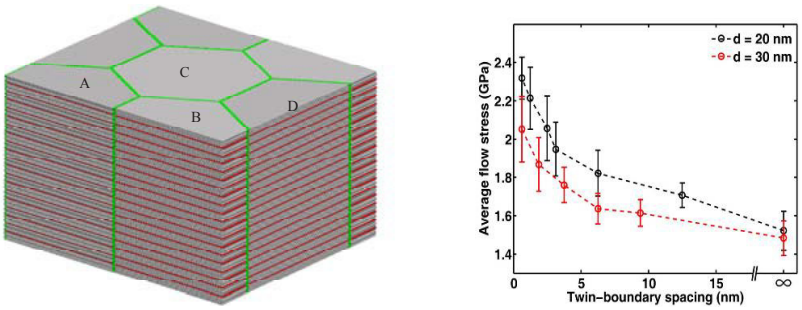

Fig. 2. Deformation and strength of nano-twinned grains via MD simulation. Left: configuration for a columnar grain with nanotwins parallel to the loading axis; right: flow stress (averaged from a true strain range of 6%–14%) versus twin-boundary spacing

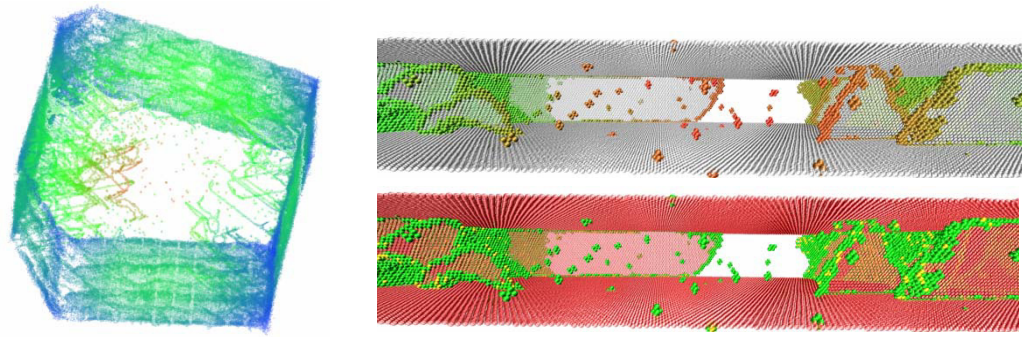

Fig. 3. The case of 5 nm twin spacing: the threading dislocations (partials) are blocked by twin boundaries. Courtesy to Xiaoyan Li and Huajian Gao for collaboration

For the case of extremely small twin-spacings, the dislocation movement parallel to the loading axis lacks driving force and ceases to operate. Another mechanism, termed extending jogs, comes into play with a configuration of chains of tiny dislocation loops. This mechanism is depicted in the left graph of Fig. 4 for the case of 1nm twin spacing. Two predictive formulas are derived for those mechanisms, as listed in the right graph of Fig. 4. The data in the graph indicate that the numerical simulation based on molecular dynamics bridges the predictions of two mechanisms.

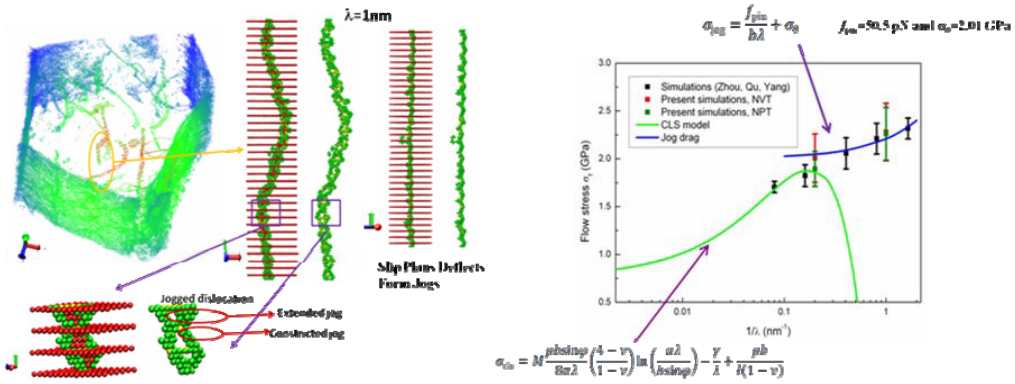

Fig. 4. Left: the mechanism of a chain of jogged dislocations for the low twin-spacing case; and right: the predictions of two mechanisms and their comparison with MD simulations. Courtesy to Xiaoyan Li and Huajian Gao for collaboration

Attention is then focused on the fracture of nanocrystals. The in-situ experiments for crack growth in nanocrystals were carried out by the Suresh group [8–10] that featured the local thinning, voiding and the coalescence of voids into the main crack. Analytic model [11] and numerical simulation [12] indicated the importance of matter diffusion along void surfaces and grain boundaries.

The objective is to perform in-situ test for crack growth in nanocrystals with atomistic resolution [13]. A special testing stage is designed to observe crack growth under HRTEM. A special holder is used with TEM. A step motor controls the loading through pin distance. The specimen was loaded in a step mode through cycles of straining and relaxing. A 20 micron-wide crevice is made on the substrate. In this region, the film is free standing. The Au thin film (30 nm in thickness) is glued on the substrate of stainless steel (25 microns in thickness). The speed of loading-pins is from 0.04 mm/s to 0.4 mm/s. We carried on the experiments using the highest elongation rate until a microcrack can be identified. Then the speed was lowered to the minimum. By loading the testing stage, the crevice opens, and that drives the propagation of the existing cracks within the free standing film. Typical atomic images of the near-tip region are illustrated in Figs. 5–7.

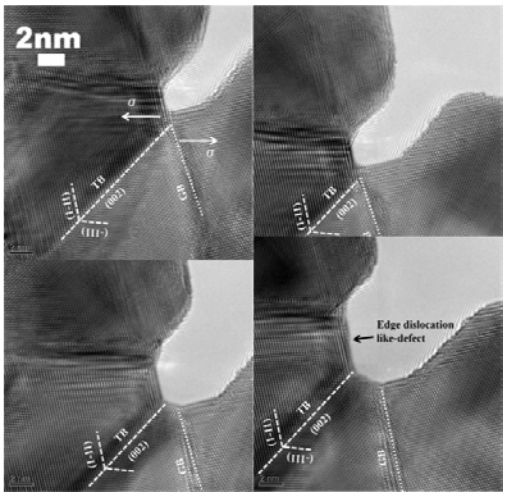

Fig. 5. Crack growth driven by surface diffusion, after Wang et al. [13]

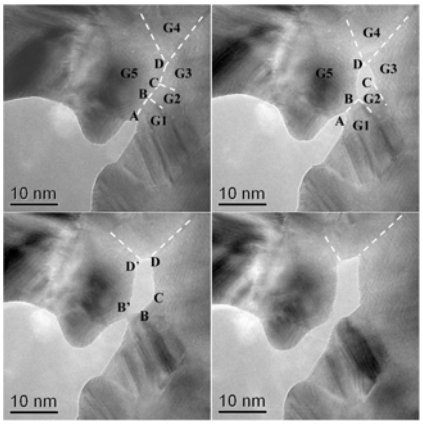

Fig. 6. Crack growth by grain boundary cavitation [13]

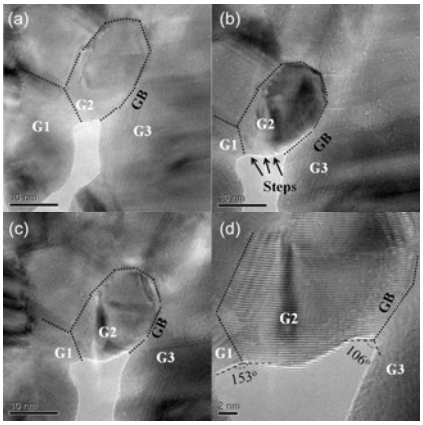

Fig. 7. Crack circumvents a grain along GB [13]

Figure 5 delineates the case of crack growth driven by atom diffusion along crack surface. Bond breakage occurs at one specific atom plane, followed by the one-by-one atom migration along the same atom plane. The process is facilitated by GB sliding which also creates the initial sites for the bond breakage.

Figure 6 illustrates another mechanism of crack growth in full atomistic details. The main crack extends into the grain boundary and nucleates a cavity ahead of the crack tip. As the crack opens and the cavity widens, the ligament starts to collapse layer-by-layer from both sides, from 9 atomic layers to 7 layers, and then to 5 layers. Eventually, the ligament ruptures and the opening void links to the main advancing crack. A different case is delineated in Fig. 7. The advancing crack is somewhat blocked by the grain of an unfavourable orientation. The crack has to circumvent the grain in both sides via grain boundaries. Diffusion in specific grain plane facilitates this process.

2. Nanomechanics of graphene

Graphene can be viewed as C atoms arranged in 2D honeycomb lattice [14]. Graphene is small, strong, stable and smart. The thickness of monolayer graphene is generally taken to be 0.34 nm. C is light, so that it has a very small electron scattering cross-section σ and bond length, which leads to difficulties in TEM imaging. Namely, small scattering cross-section leads to low contrast in TEM imaging whereas small bond length requires high resolution. To solve this problem, one has to use TEM at relatively low voltage, which gives high contrast, low damage but poor resolution. The state-of-the-art aberration-correction technique has to be used to improve the resolution.

Graphene is strongly built in every aspects. The defect-free graphene possesses excellent mechanical properties: it has a Young modulus of 1 000 GPa, an ultimate strength in the order of 100 GPa, and a specific surface area of 1 520 m^2/g. Compared to other materials commonly used for NEMS, graphene possesses an important and as-yet unexploited advantage: it can withstand ultrahigh strains, up to 25% in nanoindentation experiments and about 3%–5% for micron-sized samples subjected to uniaxial strain. Graphene can be manufactured in thin sheet and long rope [15]. Graphene can also form strong interface with two-dimensional metal. For the grapheme/ironene interface, the predicted strength is within the range of 10 – 20 GPa.

Graphene is stable. Pristine grapheme only has van der Waales interaction with many atoms. The doping atoms falling into the defects in grapheme are also very stable.

Graphene is also smart. In top-down fabricated NEMS, high resonant frequencies can be achieved by reducing the device dimensions, making it possible to detect single molecules by sensing the resonant frequency shift. The resonant frequency f is given by

$$f_{\mathrm{res}}(V_{\mathrm{g}}) = \frac{1}{2L}\sqrt{\frac{T_0 + T_{\mathrm{e}}(V_{\mathrm{g}})}{\rho w}},$$

where L and w are the length and width of the graphene sheet, ρ the density per area, V_{g} the applied voltage, and the total tension T is composed of the built-in tension T_0 and the tension caused by applied voltage $T_{\mathrm{e}}(V_{\mathrm{g}})$. Micrometer-scale graphene devices, subjected to strains of order 1%, should achieve gigahertz operation while maintaining the robust signal levels. An additional advantage is that the amplitude at the onset of nonlinearity increases with strain, so that it should be possible to simultaneously increase the frequency and dynamic range (and therefore the mass sensitivity). Such large strains are achievable by integrating graphene with MEMS/NEMS structures [16].

The nanomechanics of graphene contains the following subjects: (1) Defects and structure issues, such as controllable defect generation, structural modification, micro- and nano-fabrication. (2) Strain engineering aspects, including tune properties, band gap, and magnetic properties. (3) Strength and toughness issues, such as damage, fracture and fatigue, bearing in mind that structural integrity for graphene, either free-standing or on-substrate, is important for the next generation of NEMS. (4) Thin film mechanics, including thin film deposition (nucleation and growth kinetics), contact to metal, dielectrics, polymer and biomaterials, and large deformation in flexible electronics.

We demonstrate the nanomechanics of graphene by several examples in the following. We devise a two-step method for atomic doping of graphene: the first step consists of creating holes and vacancies in graphene by bombardment of Au atoms, while the second step consists of doping atoms of various kinds to the edges of the hole and into the atomic vacancies. These doping atoms serve to functionalize the edges and to create catalysts in the form of single atom arrays. The mechanics of graphene is explored by observing the atom-resolved mode-III fracture in graphenes, and by elucidating the failure mechanisms of graphene nano-ribbon. We are able to create a two-dimensional iron film, termed ironene, with the constraining support by graphene edges. The segregation of metallic clusters on a graphene sheet is also explored.

All TEM images reported herein were taken by using an FEI Titan TEM 80-300 microscope with both chromatic aberration and spherical aberration. The TEM was operated at 60 kV, and still with 1.1 angstrom resolution. The graphene sheet is obtained by CVD process. A two-step method for atomic doping of graphene is devised [17]. The free standing pristine graphene was set on the TEM grid. Laser was shined (400 mJ/pulse) on the target sample to trigger a plume of atom flow toward the graphene sheet, as shown in the left graph of Fig. 8. Clusters of designated atoms (with atom kinetic energy: 100 – 200 eV) bombard the graphene and leave some holes and vacancies on the graphene sheet; see the schematics in the middle graph of Fig. 8. The aftermath of the bombardment by clusters of Au atoms is shown in the right graph of Fig. 8.

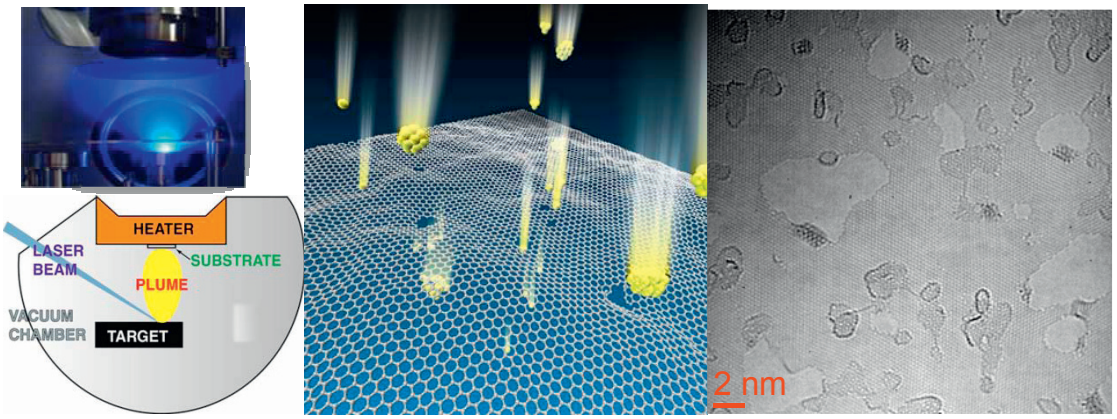

Fig. 8. Two-step doping method for atomic turnover in a graphene sheet, after Wang et al. [17]

The second step consists of doping atoms of various kinds to the edges of the hole and into the atomic vacancies. These doping atoms serve to functionalize the edges and to create catalysts in the form of single atom arrays. The doping atoms along the hole-edge is relatively stable. Relocation of the doping atom is typically achieved by a complicated collaborative movement, as exemplified in Fig. 9. Figures 9a

to 9c represent a sequence of HRTEM images illustrating the relocation of Au atom. Figure 9d provides the outline of the process, and Figs. 9e and 9f delineate the depinning process.

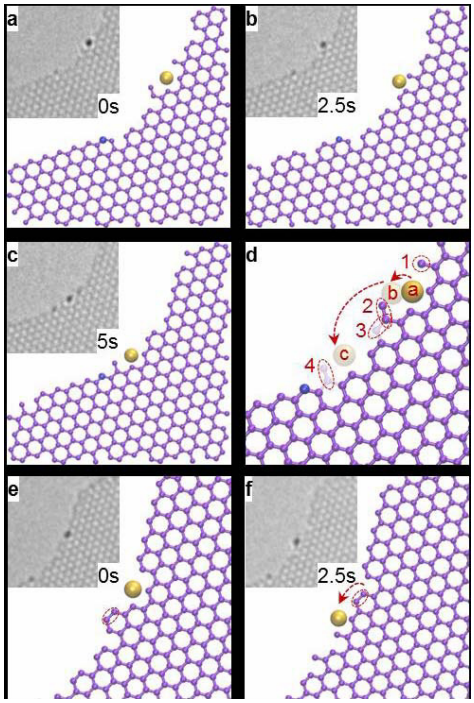

Fig. 9. Relocation of Au atom along the graphene edge [18]

The effect on atomic evolution by electron irradiation can be simulated by molecular dynamics in conjunction with the Rutherford back-scattering model [19]. Referred to Fig. 10, the transferred energy can be calculated as

$$T(\varphi) = T_{\max} \cos^2 \varphi = T_{\max} \sin^2 \frac{\theta}{2}, \qquad T_{\max} = \frac{2E\left(E + 2m_e c^2\right)}{Mc^2}.$$

The area flux can be computed by

$$\frac{\mathrm{d}\sigma}{\mathrm{d}\Omega} = \left(\frac{Ze^2}{16\pi\varepsilon_0 E}\right)^2 \sin^{-4}\frac{\theta}{2}.$$

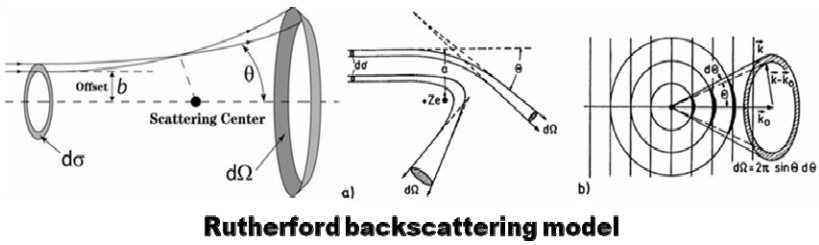

Fig. 10. Calculating electron irradiation by Rutherford backscattering model

In the above equations, m_e denotes the mass of electron, c the light velocity, Z the atomic number of the displaced atom, M the mass of atom, E=60 keV the electron energy, Ω the solid angle, θ the recoil angle and ε_0 the dielectric constant in vacuum.

The thinning of graphene nano-ribbons under electron irradiation is depicted in the left graph of Fig. 11. The nano-ribbon between the neighbouring holes becomes eroded under electron irradiation, evolved to double atom chains, and then single atom chain, and eventually collapsed. This dynamic process can be simulated according to the Rutherford backscattering model as shown in the right graph of Fig. 11. The simulation captures the essence for the rupture of the graphene nano-ribbon, aside from an accelerated effort in MD simulation.

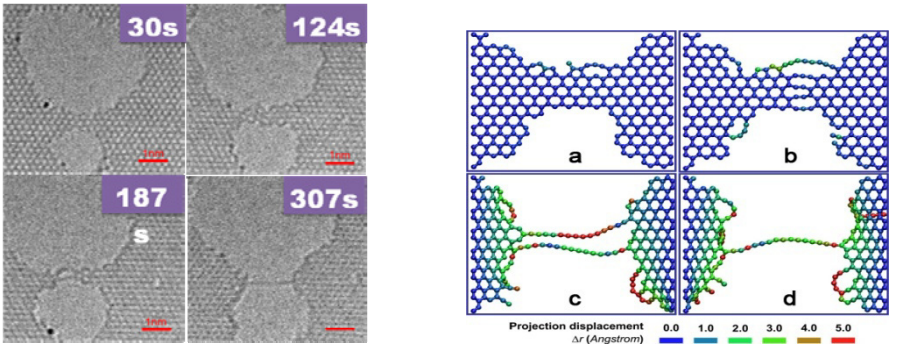

Fig. 11. Experiment and simulation for the erosion and the final rupture of graphene nano-ribbon

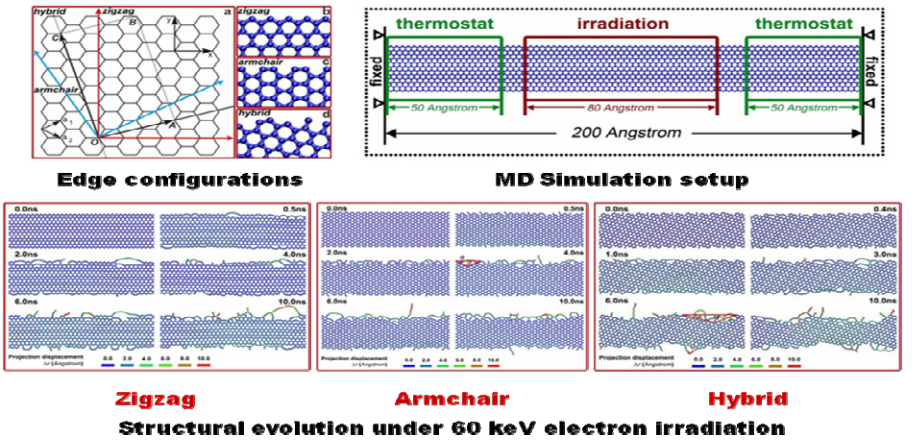

Fig. 12. Thinning of graphene nano-ribbon

The thinning of graphene nano-ribbon can be simulated by this methodology for three edge configurations: zigzag, armchair and hybrid [20]. The results indicate: (1) the zigzag edge is dynamically stable when compared with other edges, and all edges evolve to zigzag configuration; (2) the eventual roughness is dictated by the wavelength of the zigzag edge, and is of the order of 0.5 nm. That is the best attainable roughness when compared with the other methods.

Under electron irradiation, the flipped-over graphene piece may proceed to tear, as observed in the experiment. This process is depicted at the central upper sketch of Fig. 13, resembling the experimental

snapshots in the same figure. The tearing process is envisaged as follows. The folded graphene sheet causes two consequences. First, the pressure on the folded part is roughly doubled by offering more scattering area in electron irradiation, leading to stress concentration at the root of the folding graphene, and resulting in the breakage of the atomic bonds. Second, the folding is energetically favourable if one compares the energy balance from two surfaces to a folded interface. Accordingly, a long range driving force appears that pulls the flipped-over sheet to further cover the underneath graphene. The experiment clearly indicates that the tearing process (or mode III fracture process) is brittle. The process only induces bond breaking and local elastic distortion. The extended defect propagation, such as 5-7-7-5 SW defect, cannot be observed.

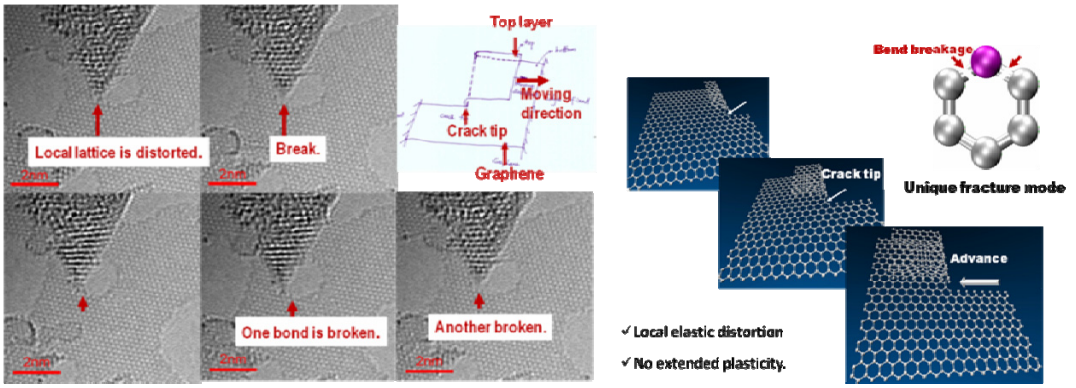

Fig. 13. Tearing of a grapheme: experiment snapshots, mechanism sketch, and MD simulation

3. Nanocrystals on graphene

Nanocrystals may interact in various ways with a supporting graphene sheet. We demonstrate this interaction by three examples: (1) ultrafine Fe cluster along graphene edge under electron irradiation; (2) edge supported 2-D iron film by graphene; (3) three-dimensional Pt cluster on graphene.

Let first consider structure evolution of an ultrafine Fe cluster under electron irradiation, as shown in Fig. 14. Figures 14a to 14f exhibit the sequence of aberration-corrected TEM image of a cluster sitting on a graphene support, which is divided into two regions with monolayer and bilayer. The Fe nanocrystal takes the shape of a three-layer triangle. The white dashed line delineates the boundary in Fig. 14b with a scale bar of 1 nm. The arrow heads in Figs. 14e and 14f indicate a single Fe atom trapped on the edge. The cluster in Fig. 14f, as indicated by the white arrow, encounters the adsorbate on graphene. Their merge leads to a cluster that no longer retains its shape of a regular triangle. Figure 14 provides an atomic model of the cluster with 53 atoms in a three-layer hexagonal close-packed structure. Corresponding TEM simulations of the model are presented in Figs. 14h and 14i by using the software MacTempasX incorporated with the multislice method. Two graphs refer to the situations with and without a monolayer graphene support.

The second case is for two-dimensional iron crystals assembled on graphene edge. The thin Fe film with a single layer of atoms is termed ironene. It was claimed long ago that metal cluster cannot take two-dimensional form above absolute zero temperature without external support. Thin metallic film can be deposited on a substrate. One may further explore the possibility of supporting two-dimensional crystal by constraining its edge, such as the case of forming water membrane by a thin-wired support, as shown in Fig. 15a. With the hole perimeter of graphene as the supporting edge, a single layer of metallic atoms may be stabilized in two-dimensional shape. Indeed the TEM image in Fig. 15b reveals a junction

bridging two graphene edges, which is assembled by monolayer iron atoms. Figure 15c shows a 2D iron crystal embedded in graphene lattice, with a scale bar of 0.5 nm. Figure 15d gives the atomic model and TEM simulations of a 2D iron crystal, in agreement with the ironene configuration. DFT calculations reveal that the unit cell only has two-fold symmetry and lattice constants of a = 2.5 Å and b = 4.1 Å. The epitaxial directions are labelled in the corresponding lattice coordinate. Atomic models and TEM simulations of iron crystals with Fig. 15e two and Fig. 15f three close-packing layers as sequenced in the face-centered cubic lattice are also illustrated in Fig. 15.

Our final example deals with Pt clusters on a graphene sheet. The left four graphs of Fig. 16 portray the evolution of Pt clusters at the graphene edge under 60 kV electron irradiation. The Pt cluster takes a three dimensional shape of truncated octahedron. The right graph of Fig. 16 proposes a model of truncated octahedron in an FCC crystal coordinate system, complemented with two snapshots of crystal 3 with the atomic model viewed along different directions.

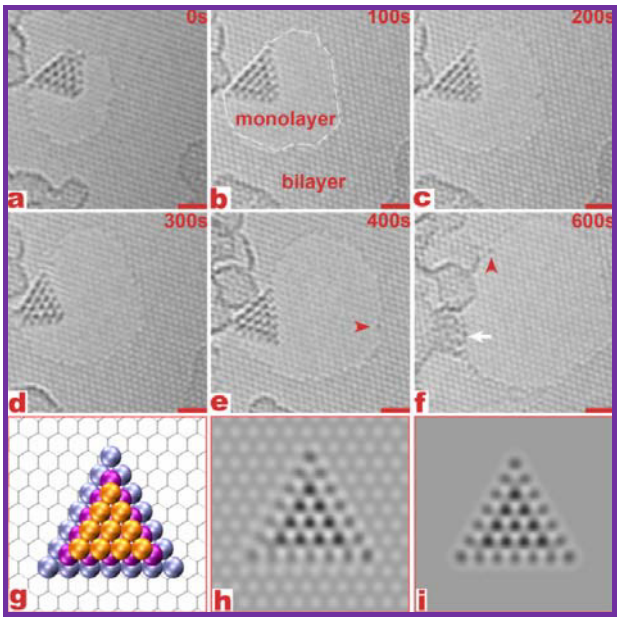

Fig. 14. Triangular iron cluster on graphene

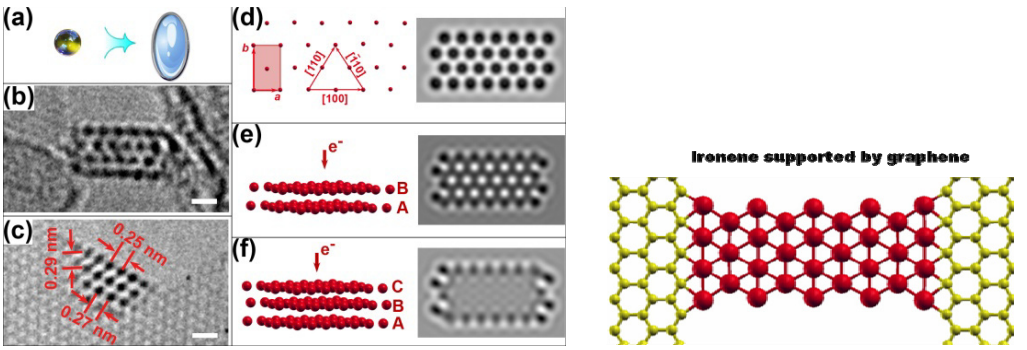

Fig. 15. The observation and simulation of ironene

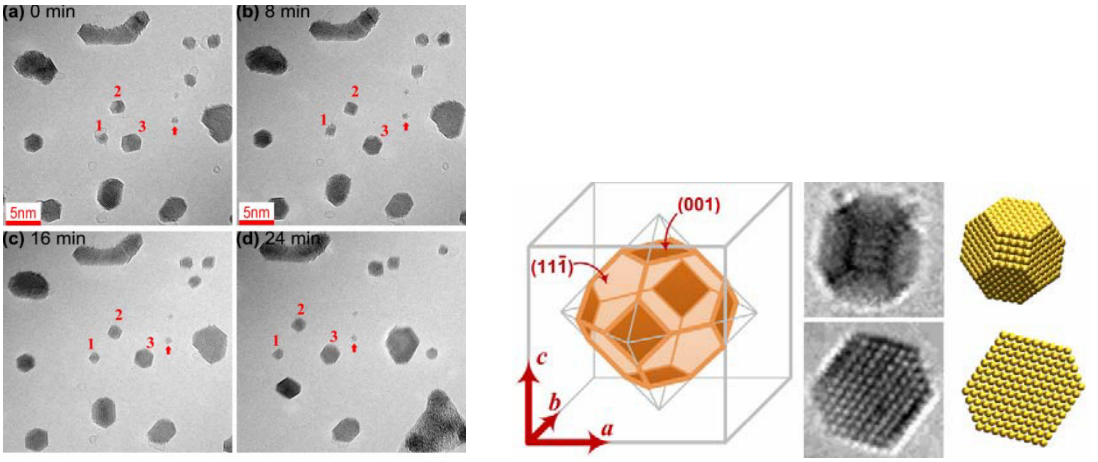

Fig. 16. Observation of Pt cluster at the graphene edge and the atomic model for truncated octahedron

4. Conclusions

The following conclusions are arrived:

(1) Deformation and fracture of nanocrystals are dominated by diffusion processes.
(2) Different atoms can be doped into graphene by using a two-step method of atomic turnover.
(3) Graphene nano-ribbons can be tailored by electronic irradiation.
(4) Graphene is intrinsically brittle. The tearing process proceeds by bond breaking and continued folding.
(5) Surface and hole perimeter of graphene provide support for metallic atoms and low dimensional nanocrystals.

Acknowledgements

We acknowledge Advanced Nanofabrication, Imaging and Characterization Core Lab in King Abdullah University of Science and Technology for characterization facilities. This work has been supported by the National Science Foundation of China (10832009 and 11090333) and Science Foundation of Chinese University (2011QNA4038). The computational work carried out by TianHe-1(A) system at National Supercomputer Center in Tianjin, China is gratefully acknowledged.

References

[1] Lu L, Sui ML, Lu K. Superplastic extensibility of nanocrystalline copper at room temperature. *Science* 2000; **287**: 1463–1466.
[2] Yang W, Wang HT. Mechanics modeling for deformation of nano-grained metals. *J Mech Phys Solids* 2004; **52**: 875–889.
[3] Wang HT, Yang W. Constitutive modeling for nanocrystalline metals based on cooperative grain boundary mechanisms. *J Mech Phys Solids* 2004; **52**: 1151–1173.
[4] Yang W, Ma XL, Wang H, Hong W. Progresses in nano-mechanics. *Advances in Mechanics* 2002; **32**: 161–174.
[5] Lu K, Lu L, Suresh S. Strengthening materials by engineering coherent internal boundaries at the nanoscale. *Science* 2009; **324**: 349.
[6] Li XY, Wei Y, Lu L, Lu K, Gao H. Dislocation nucleation governed softening and maximum strength in nano-twinned metals.

Nature 2010; **464**: 877–880

[7] Zhou HF, Qu SX, Yang W. Toughening by nano-scaled twin boundaries in nanocrystals. *Mod Simul Mater Sci Engng* 2010; **18**: 065002.

[8] Kumar KS. Suresh S. Chisholm MF, Horton JA, Wang P. Deformation of electrodeposited nanocrystalline nickel. *Acta Mater* 2003; **51**: 387–405.

[9] Kumar KS, Van Swygenhoven H, Suresh S. Mechanical behavior of nanocrystalline metals and alloys. *Acta Mater* 2003; **51**: 5743–5774.

[10] Lu L, Schwaiger R, Shan ZW, Dao M, Lu K, Suresh S. Nano-sized twins induce high rate sensitivity of flow stress in pure copper. *Acta Mater* 2005, **53**: 2169–2179.

[11] Yang F, Yang W. Brittle versus ductile transition of nanocrystalline metals. *Int J Solids Structs* 2008; **45**: 3897–3907.

[12] Yang F, Yang W. Crack growth versus blunting in nanocrystalline metals with extremely small grain size. *J Mech Phys Solids* 2009; **57**: 305–324.

[13] Wang HT, Nie AM, Liu JB, Wang P, Yang W, Chen BD, et al. In situ TEM study on crack propagation in nanoscale Au thin films. *Scripta Materialia* 2011; **65**: 377–379.

[14] Geim AK, Novoselov KS. The rise of graphene. *Nat Mater* 2007; **6**: 183–191.

[15] Xu Z, Gao C. Graphene chiral liquid crystals and macroscopic assembled fibres. *Nat Commun* 2011; 2: 571.

[16] Chen C, Rosenblatt S, Bolotin KI, Kalb W, Kim P, Kymissis I, et al. Performance of monolayer graphene nanomechanical resonators with electrical readout. *Nat Nano* 2009; **4**: 861–867.

[17] Wang HT, Wang QX, Cheng YC, Li SK, Yao YB, Zhang Q, et al, Doping Monolayer Graphene with Single Atom Substitutions. *Nano Letters* 2012; **12**: 141–144.

[18] Wang HT, Li K, Cheng YC, Wang Q, Yao Y, Schwingenschlögl U, et al. Interaction between single gold atom and the graphene edge: A study via aberration-corrected transmission electron microscopy. *Nanoscale* 2012; **4**: 2920–2925.

[19] Kohl H, Reimer L. *Transmission Electron Microscopy: Physics of Image Formation*. New York: Springer, 1997.

[20] Zhu WP, Wang HT, Yang W. Evolution of graphene nanoribbons under low-voltage electron irradiation. *Nanoscale* 2012; **4**: 4555–4561.